AGU PUBLICATIONS

JGR

Journal of Geophysical Research: Space Physics

RESEARCH ARTICLE

10.1002/2016JA022787

Key Points:
- Occurrence rate of FRs and RFs at Mercury is ~60 times higher than at Earth, due to the variable magnetospheric conditions at Mercury
- Magnetic reconnection occurs more frequently in the dawnside than in the duskside in Mercury's plasma sheet, opposite to Earth's results
- Plasma flows would brake and initiate dipolarizations on the postmidnight sector at Mercury different to the premidnight locations at Earth

Correspondence to:
W. J. Sun,
weijiesun@pku.edu.cn

Citation:
Sun, W. J., S. Y. Fu, J. A. Slavin, J. M. Raines, Q. G. Zong, G. K. Poh, and T. H. Zurbuchen (2016), Spatial distribution of Mercury's flux ropes and reconnection fronts: MESSENGER observations, *J. Geophys. Res. Space Physics*, *121*, 7590–7607, doi:10.1002/2016JA022787.

Received 4 APR 2016
Accepted 19 JUL 2016
Accepted article online 22 JUL 2016
Published online 13 AUG 2016

Spatial distribution of Mercury's flux ropes and reconnection fronts: MESSENGER observations

W. J. Sun[1,2], S. Y. Fu[1], J. A. Slavin[2], J. M. Raines[2], Q. G. Zong[1], G. K. Poh[2], and T. H. Zurbuchen[2]

[1]School of Earth and Space Sciences, Peking University, Beijing, China, [2]Department of Climate and Space Sciences and Engineering, University of Michigan, Ann Arbor, MI, USA

Abstract We perform a statistical study of flux ropes and reconnection fronts based on MErcury Surface, Space ENviroment, GEochemistry, and Ranging (MESSENGER) magnetic field and plasma observations to study the implications for the spatial distribution of reconnection sites in Mercury's near magnetotail. The results show important differences of temporal and spatial distributions as compared to Earth. We have surveyed the plasma sheet crossings between $-2\,R_M$ and $-3\,R_M$ downtail from the planet, i.e., the location of Near-Mercury Neutral Line (NMNL). Plasma sheets were defined to be regions with $\beta \geq 0.5$. Using this definition, 39 flux ropes and 86 reconnection fronts were identified in the plasma sheet. At Mercury, the distributions of flux ropes and reconnection fronts show clear dawn-dusk asymmetry with much higher occurrence rate on the dawnside plasma sheet than on the duskside. This suggests that magnetic reconnection in Mercury's magnetotail occurs more frequently in the dawnside than in the duskside plasma sheet, which is different than the observations in Earth's magnetotail showing more reconnection signatures in the duskside plasma sheet. The distribution of plasma sheet thickness shows that plasma sheet near the midnight is the thinnest part and does not show obvious asymmetry. Thus, the reasons that cause magnetic reconnection to preferentially occur on the dawnside of the magnetotail at Mercury may not be the plasma sheet thickness and require further study. The peak occurrence rates of flux ropes and reconnection fronts in Mercury's plasma sheet are ~60 times higher than that of Earth's values, which we interpret to be due to the highly variable magnetospheric conditions at Mercury. Such higher occurrence rate of magnetic reconnection would generate more plasma flows in the dawnside plasma sheet than in the duskside. These plasma flows would mostly brake and initiate the substorm dipolarization on the postmidnight sector at Mercury rather than the premidnight susbtorm onset location at Earth.

1. Introduction

Mercury is the closest to the Sun of the planets in the Solar System, with solar wind conditions quite different than those near Earth. Because the solar wind velocity does not vary a lot from Mercury to Earth, the stronger interplanetary magnetic field (IMF) intensity and higher solar wind density at Mercury would result in higher solar wind dynamic pressure than that at Earth [e.g., *Glassmeier*, 1997]. Observations from Mariner 10 and MErcury Surface, Space ENviroment, GEochemistry, and Ranging (MESSENGER) [*Solomon et al.*, 2007] revealed that Mercury's intrinsic magnetic field is closely aligned (<5°) with the planet's rotation axis and exhibits the same polarity as the Earth, but the intensity of magnetic field near Mercury's surface is only ~1% of the Earth's surface field [e.g., *Ness et al.*, 1974; *Alexeev et al.*, 2010; *Anderson et al.*, 2010, 2011]. It is because of the strong solar wind dynamic pressure and weak internal magnetic field that the subsolar standoff distance for Mercury's magnetopause is only $\sim 0.45\,R_M$ away from the surface, where $R_M \approx 2440$ km is Mercury's radius [*Winslow et al.*, 2013; *Zhong et al.*, 2015]. Mercury's magnetosphere has been reported to be experienced by many similar processes and structures dominated by magnetic reconnection as those at Earth, such as the flux transfer events (FTEs) near the magnetopause [*Russell and Walker*, 1985; *Slavin et al.*, 2009, 2010a, 2012a], flux ropes and reconnection fronts in the magnetotail [*Slavin et al.*, 2009, 2012b; *Sundberg et al.*, 2012a; *DiBraccio et al.*, 2015], and also the magnetospheric substorm processes [*Slavin et al.*, 2010b; *Sun et al.*, 2015a, 2015b]. Mercury's magnetospheric substorm at Mercury exhibits similar plasma sheet thinning process during growth phase and plasma sheet thickening during expansion phase, i.e., magnetospheric global reconfiguration during substorm [*Sun et al.*, 2015b] but with a time scale (~2 to 3 min) much shorter than Earth's substorm (~2 to 3 h) [*Slavin et al.*, 2010b; *Sun et al.*, 2015b].

Plasmoids were first proposed to be formed between the near and distant neutral lines during Earth's substorms with magnetic loop structures [*Hones*, 1977]. In order to generate magnetic loop topology, it would

require antiparallel (~180°) magnetic field lines between the neutral lines in the magnetotail. But the magnetic field in Earth's magnetotail is commonly observed to have strong B_y with the influence of IMF [e.g., *Cowley*, 1981]. This strong B_y would result in the formation of flux ropes containing helical field lines between neutral lines [e.g., *Hughes and Sibeck*, 1987; *Moldwin and Hughes*, 1991]. The motion of plasmoids or flux ropes in the plasma sheet could compress the nearby lobe regions, which are called traveling compression regions (TCRs) [*Slavin et al*., 1984]. Reconnection fronts (RFs, also called dipolarization fronts) were extensively studied in the Earth's plasma sheet [*Runov et al*., 2009; *Angelopoulos et al*., 2013; *Liu et al*., 2013; *Sun et al*., 2013] and are believed to be highly associated with magnetic reconnection [e.g., *Sitnov et al*., 2009; *Fu et al*., 2013; *Ashour-Abdalla et al*., 2015]. The structure is identified as the leading edge of planetward propagating dipolarizing flux bundle (DFB, also called plasma bubble) [*Liu et al*., 2013; *Sun et al*., 2014]. The distributions of flux ropes, reconnection fronts, and TCRs in Earth's magnetotail show clear dawn-dusk asymmetry with more events observed on the duskside than on the dawnside [*Slavin et al*., 2005; *Imber et al*., 2011; *Liu et al*., 2013], which indicate that magnetic reconnection would more frequently occur in the duskside plasma sheet. This indication agrees with the distribution of reconnection generated flux bursts [e.g., *Angelopoulos et al*., 1994; *Raj et al*., 2002] and also the detected reconnection diffusion regions [e.g., *Nagai et al*., 2013, 2015; *Genestreti et al*., 2014] at Earth.

Employing the observations from MESSENGER, *Slavin et al*. [2012b] and *DiBraccio et al*. [2015] studied the plasmoids, flux ropes, and TCRs in Mercury's magnetotail. *Slavin et al*. [2012b] showed that plasmoids had the durations of ~ 1 to 3 s and diameters of 500 to 1500 km. *DiBraccio et al*. [2015] conducted a statistical survey of flux ropes in Mercury's plasma sheet. Flux ropes were fitted to a force-free model, and the mean radius of them (~480 km) was shown to be comparable with the background proton gyroradius (~380 km) indicating kinetic effects might be important for the flux ropes. *DiBraccio et al*. [2015] constrained the flux ropes in the region of 0.5 R_M centered at midnight and therefore did not exhibit the dawn-dusk distribution of flux ropes. *Sundberg et al*. [2012a] carried out a study of reconnection fronts and DFBs in Mercury's magnetotail, which contained only five plasma sheet crossings from MESSENGER's orbits. In their study, reconnection fronts were observed to be well-defined one-dimensional current sheets, which is consistent with the Earth's study [*Runov et al*., 2009; *Liu et al*., 2013; *Sun et al*., 2014]. But the reconnection fronts and DFBs in Mercury's magnetotail only lasted ~ 2 s and ~ 10 s in average, respectively, which are shorter than those structures in Earth's plasma sheet [e.g., *Liu et al*., 2013]. The relative short timescales of reconnection fronts and DFBs in Mercury's plasma sheet might reveal the plasma environment at Mercury is different to that at Earth.

Because of the high correlation between these structures (i.e., flux ropes and reconnection fronts in the plasma sheet) and magnetic reconnection, a larger statistical study of flux ropes and reconnection fronts could help us to understand the features of magnetic reconnection in Mercury's plasma sheet, especially the dawn-dusk distributions. The comparison with Earth's results would also increase our understanding of the dynamic processes in Mercury's magnetosphere. By using MESSENGER's magnetic field and plasma data, we have performed such a statistical survey of flux ropes and reconnection fronts in Mercury's magnetotail. We show the occurrence rates and dawn-dusk distribution of these structures and discuss the near-tail reconnection distributions at Mercury. We also compare the results with Earth's.

2. Data Sources

This study utilizes plasma and magnetic field data from MESSENGER instruments. The fast imaging plasma spectrometer (FIPS) sensor [*Andrews et al*., 2007] measures ions with an energy range from 50 eV/e to 13.7 keV/e in 10 s energy scan. FIPS had a field of view ~ 1.4 π sr and an angular resolution of ~ 15°. Ion moments (density and temperature) can be derived from average FIPS spectra under the assumption of nearly isotropic and highly subsonic plasma [*Raines et al*., 2011; *Gershman et al*., 2013]. In this work, plasma moments obtained from 1 min averaged spectra in the magnetotail are used. The magnetometer (MAG) [*Anderson et al*., 2007] provides magnetic field measurements at a sample rate of 20 vectors per second. Magnetic field is given in the Mercury Solar Magnetospheric (MSM) coordinates. This coordinate system is centered on the Mercury's magnetic dipole, which has a ~ 0.2 R_M offset northward of the planet's center [e.g., *Alexeev et al*., 2010; *Anderson et al*., 2010]. In the coordinates, X_{MSM} axis is sunward, Z_{MSM} axis is northward and normal to the magnetic equatorial plane, and Y_{MSM} axis completes the right-handed coordinate system. Spacecraft position data are provided with the same resolution as magnetic field data and also in

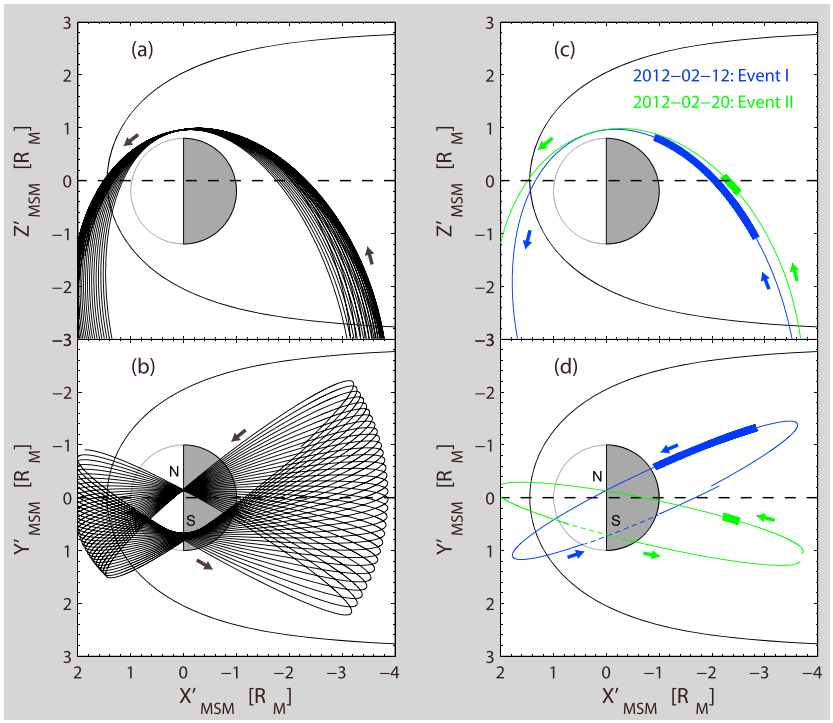

Figure 1. (a, b) MESSENGER orbits during the hot season from 9 February 2012 to 23 February 2012 in the MSM′ *X′Z′* and *X′Y′* planes, respectively. (c, d) Two orbits from one of the MESSENGER's hot season on 12 February 2012 (blue lines, Event I) and 20 February 2012 (green lines, Event II) in the MSM′ *X′Z′* and *X′Y′* planes, respectively. The thick portions in each orbit indicate the regions where MESSENGER was located in the plasma sheet.

the MSM coordinates. We have transformed the spacecraft position into aberrated MSM coordinate system (MSM′) in which X'_{MSM} is antiparallel to the average solar wind flow (~400 km/s); i.e., X_{MSM} and Y_{MSM} have been rotated according to Mercury's orbital motion and average solar wind velocity [e.g., *Johnson et al.*, 2012].

MESSENGER was inserted into orbit about Mercury on 18 March 2011. It entered into a highly eccentric orbit (~200 km × ~ 15 300 km) with an inclination of 82.5° until 16 April 2012 when the apoapsis of the orbit was reduced to ~ 10,000 km and the orbital period was changed from ~ 12 h to ~ 8 h. MESSENGER's orbits could be divided into "hot" and "warm" seasons during which the MESSENGER periapsis was located on the dayside and nightside, respectively. The positions where MESSENGER crossed the plasma sheet during hot season orbits were further downtail than the warm season orbits, which were resulted from the different periapsis locations. Before 16 April 2012, MESSENGER crossed the plasma sheet at a distance of ~ $-2\ R_M$ to $-3\ R_M$ downtail during hot seasons, which is consistent with the location of Near-Mercury Neutral Line (NMNL) [*Slavin et al.*, 2012b; *DiBraccio et al.*, 2015]. Previous studies at Earth have revealed that the distributions of flux ropes [*Imber et al.*, 2011] and reconnection fronts [*Zhou et al.*, 2014] earthward of the Near-Earth Neutral Line (NENL, $> -20\ R_E$) is different to that in the NENL region. In order to remove this effect, we therefore only study the flux ropes and reconnection fronts in the NMNL region and also investigate the feature of Mercury's near tail reconnection site. In this study, we survey the plasma sheet crossings during the hot seasons before 16 April 2012. There are three hot seasons, which are from 17 August 2011 to 3 September 2011, 13 November 2011 to 29 November 2011, and 9 February 2012 to 23 February 2012. Figures 1a and 1b show the spatial distribution of orbits in MSM *X′*-*Z′* and *X′*-*Y′* planes for the hot season from 9 February 2012 to 23 February 2012. It can be seen that MESSENGER's orbits are evenly distributed in the magnetotail during this hot season without obvious bias.

3. Observations of Plasma Sheet

3.1. MESSENGER Observations

Figures 1c and 1d depict two MESSENGER's orbits containing two plasma sheet crossings from one of the three hot seasons. During the intervals, MESSENGER entered into the southern lobe of the tail at the beginning

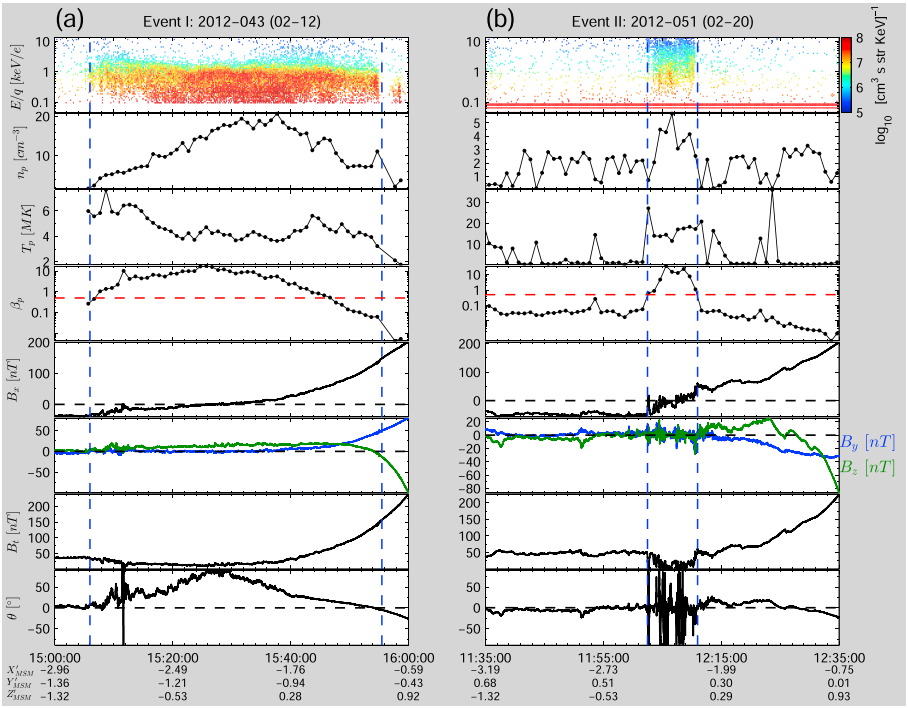

Figure 2. Plasma and magnetic field measurements taken from MESSENGER during plasma sheet crossings for (a) Event I (12 February 2012) and (b) Event II (20 February 2012). From the first panel to eighth panel in both Figures 2a and 2b show proton energy spectrum; proton density; proton temperature; plasma β, $\beta_p = n_p k_B T_p / \left(B_t^2/2\mu_0\right)$ (red horizontal lines indicate $\beta_p = 0.5$); magnetic field X component (B_x, in nT); magnetic field Y and Z components (B_y and B_z, in nT); magnetic field intensity (B_t, in nT); and magnetic elevation angle (θ), $\theta = \arctan\left(B_z/\sqrt{B_x^2 + B_y^2}\right)$. Beneath Figures 2a (eighth panel) and 2b (eighth panel), the ticks are labeled with UT, X'_{MSM}, Y'_{MSM}, and Z'_{MSM}. Vertical dashed lines mark the boundary of plasma sheet as determined from the energy spectra.

(Figure 1c) and then crossed the equatorial region and moved into the northern lobe of the near tail. The orbits on 12 February 2012 (in blue, Event I) and 20 February 2012 (in green, Event II) crossed the dawnside and duskside plasma sheet in the tail, respectively. Figure 2 shows the plasma and magnetic field measurements from the two plasma sheet crossings. Vertical dashed lines mark the boundaries of plasma sheet for both events, which are defined to be the edges of high particle flux regions. The regions between two vertical dashed lines correspond to the thick portions on orbital trajectories in Figures 1c and 1d. B_x is negative and B_t almost constant (~40 nT for Event I and ~ 50 nT for Event II) before the first vertical lines in both events, indicating MESSENGER was located in the southern lobe. This was confirmed by plasma observation in Figure 2 showing tenuous particles during the intervals for both events. For both events, increasing particle flux at the first vertical lines, which are defined as the southern edges of plasma sheets, indicates that MESSENGER entered into the plasma sheet. The high proton number density ($n_p > 1\ cm^{-3}$), depression in B_t, increase in plasma β and magnetic elevation angle (θ) are consistent with features of the plasma sheet. The north boundaries of plasma sheet after the crossing of neutral sheet (reverses in B_x) for both events are marked by the second vertical dashed lines. The north boundary in Event II is located at ~ [−2.19, 0.35, 0.11] R_M, but plasma observations for Event I show that MESSENGER was still in the plasma sheet until ~ 15:56:00 UT when spacecraft was located at ~ [−0.94, −0.59, 0.81] R_M indicating it encountered the high-latitude, low-altitude plasma sheet. Magnetic field intensity is much higher in the high-latitude plasma sheet than the further downtail plasma sheet (as shown in Event I). Therefore, we will exclude the high-latitude, low-altitude plasma sheet regions in this study. The durations in Figure 2 for both events are 1 h. These plasma sheet observations indicate that the plasma sheet thicknesses for the two crossings are distinct. We then estimate the thicknesses of the plasma sheets from the locations of spacecraft during the plasma sheet crossing for both events.

In order to avoid the influence from high-latitude, low-altitude plasma sheets in the northern hemisphere, we only determine the half thickness of plasma sheet in the southern hemisphere. MESSENGER crossed the

south edges of plasma sheet at ~ [−2.83, −1.32, −1.07] R_M and ~ [−2.49, 0.44, −0.22] R_M for Event I and Event II, respectively. The centers of the neutral sheets determined from the reverse in B_x during the plasma sheet crossings were at ~ [−2.24, −1.13, −0.21] R_M and ~ [−2.40, 0.41, −0.12] R_M for the two events. Thus, the half thicknesses of plasma sheet for Event I and Event II are ~ 0.86 R_M and ~ 0.1 R_M, respectively, which is deemed to be the difference between the south boundary of plasma sheet and the center of the neutral sheet. It needs to be noted that there could be multiple neutral sheet crossings (i.e., many B_x reversals) during one plasma sheet crossing. In this study, the center of neutral sheet is determined as the average position of the first and last B_x reversals similar to the study of *Zhang et al*. [2016]. The results show that the half thickness for Event I is about an order of magnitude (~8.6 times) thicker than Event II suggesting that the plasma sheet thickness could be extremely variable at Mercury. The proton density and temperature were ~ 5 cm^{-3} and ~ 15 MK for Event II but were much denser (~15 cm^{-3}) and cooler (~4 MK) for Event I, which shows that thick plasma sheet contains denser and cooler plasma than the thin plasma sheet. In Event II, the proton gyroradius was estimated to be in the range of 200 to 700 km, which is comparable to the determined plasma sheet thickness (~0.2 R_M, ~ 488 km). Therefore, we would expect intense kinetic effects in this plasma sheet, which is confirmed by the fluctuations in magnetic field B_z and elevation angle shown in Figure 2. While in Event I, the proton gyroradius was estimated to be in the range of 100 to 300 km, which is 10 times smaller than the plasma sheet thickness (~1.72 R_M, ~ 4200 km).

3.2. Plasma Sheet Identification

In previous studies of the Earth's plasma sheet, the magnetic elevation angle (θ) [e.g., *Baumjohann et al*., 1990] and plasma β [e.g., *Angelopoulos et al*., 1994] were commonly used in the separation of plasma sheet and lobes. In the lobe regions, B_x (sometimes B_y could be comparable with B_x) is generally much larger than B_z,, and therefore, the magnetic elevation angle is small. As shown in Figure 2, θ is smaller than 15° in the southern lobes of both events but is much higher in the plasma sheet. In addition, the lobe region contains tenuous plasma leading to a small plasma thermal pressure ($n_i k_B T_i + n_e k_B T_e$) and plasma β. But in the plasma sheet, plasma thermal pressure would be comparable or much larger than the magnetic pressure. Subsequently, plasma β should be close to or much higher than one, which has been also confirmed in Event I and Event II.

In this study, we use plasma β_p (the ratio of proton thermal pressure to magnetic pressure) as the indicator to separate the plasma sheet and lobe. MESSENGER did not carry an instrument to measure low-energy electron distributions, but the statistical results in Earth's plasma sheet had revealed that ion thermal pressure is commonly several times (~5 to 10) larger than electron thermal pressure [e.g., *Baumjohann et al*., 1989], and the main ion species is proton (>90%) in Mercury's plasma sheet [*Gershman et al*., 2014]. Therefore, plasma β_p should be pretty close to plasma β. We have employed both the plasma β_p and the magnetic elevation angle as the criteria to separate the plasma sheet and lobe.

Figure 3 shows the samples of θ and β_p during the three hot seasons in the magnetotail regions containing 98 orbits. The magnetotail crossings with particles from magnetosheath, which contain higher particle flux and lower energy than the plasma sheet particles [e.g., *Zurbuchen et al*., 2011], were excluded. The magnetotail data points are also constrained to be in the regions within $-1.0\,R_M < Z_{MSM} < 0.4\,R_M$. $Z_{MSM} < 0.4\,R_M$ is used to remove the data points in high-latitude, low-altitude plasma sheet. Both θ and β_p are in 1 min resolution, where magnetic field data are 1 min averaged according to the duration of plasma data. Most of the samples in small β_p region correspond with times of small θ (<20°), which should be the lobe samples. The high β_p region incorporates most of the high θ samples, which is consistent with the features in plasma sheet. In order to find the plasma β_p corresponded to the boundary between plasma sheet and lobe, we have shown the average value of θ ($\overline{\theta}$, stars) and the corresponded standard deviation (bars) for each β_p bin in the figure. The value of $\overline{\theta}$ shows a clear jump around $\beta_p = 0.4$ to 0.5. In the bin of $\beta_p = 0.5$, $\overline{\theta} \approx 14.5°$ with a standard deviation of 15.0°, and in the bin of $\beta_p = 0.4$, $\overline{\theta} \approx 10.3°$ with a standard deviation of 10.7°. Thus, we define that $\beta_p \geq 0.5$ corresponds to the plasma sheet region and $\beta_p < 0.5$ the lobe region. We take Event I (Figure 2a) and Event II (Figure 2b) as examples to evaluate this criterion. The horizontal lines in the β_p panels indicate that $\beta_p = 0.5$ generally coincide with the boundaries of plasma sheet for both events except the high-latitude plasma sheet boundary in Event I. In Event I, the south boundary of plasma sheet was located between the points of $\beta_p = 0.1$ (in the lobe side) and 0.5 (in the plasma sheet side). In Event II, $\beta_p = 0.62$ and 1.01 in the plasma sheet side and $\beta_p = 0.08$ and 0.06 in the lobe side for the two vertical dashed lines, respectively.

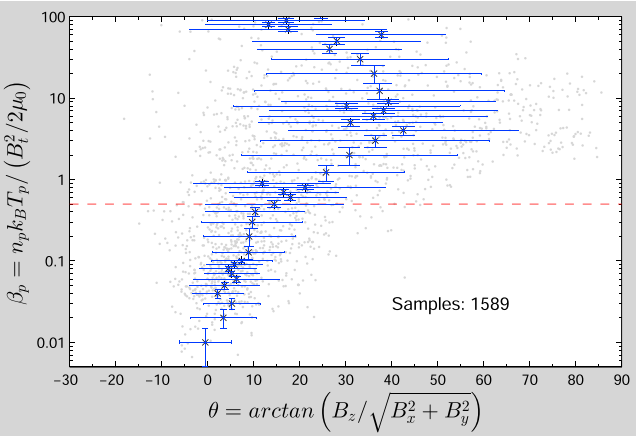

Figure 3. Scatterplot of the magnetic elevation angle (θ) and plasma β_p when MESSENGER was in the magnetotail during the three hot seasons. Both θ and β_p are in 1 min resolution. Gray dots represent data points. The averaged value of θ and the corresponded standard deviation in each β_p bin are shown as the asterisk and blue lines. Red dashed line marks the bin of $\beta_p = 0.5$.

Observations from both of the events verify that $\beta_p \geq 0.5$ can be used to identify the plasma sheet. It needs to note that the boundary of high-latitude plasma sheet in Event I is not consistent with the criterion $\beta_p \geq 0.5$. In this study, we only use $\beta_p \geq 0.5$ to determine the south boundaries of plasma sheets. During the hot seasons, MESSENGER always crossed the south boundaries of plasma sheet at a distance downtail further than $-2\,R_M$.

4. Observations of Flux Ropes and Reconnection Fronts

4.1. Flux Rope Selection

Flux ropes could be formed between pairs of reconnection sites and are proved to have helical magnetic field topologies [*Moldwin and Hughes*, 1992; *Lepping et al*., 1995]. In the magnetotail, strong core fields are observed inside the flux ropes in dawn-dusk direction, which are believed to be highly related with large IMF B_y [*Slavin et al*., 2003, 2005]. Both planetward and tailward traveling flux ropes were reported in the Earth's and Mercury's magnetotail [*Moldwin and Hughes*, 1994; *Slavin et al*., 2003, 2012b; *Zong et al*., 2004; *DiBraccio et al*., 2015]. Figures 4a and 4b show two examples of planetward traveling flux rope (PFR) and tailward traveling flux rope (TFR) observed by MESSENGER in Mercury's plasma sheet. From this figure, we can see that the most prominent signatures for flux ropes are clearly south-then-north (SN, for PFR) or north-then-south (NS, for TFR) bipolar in the B_z component, which are accompanied by the enhancements in B_y and B_t. The maximum B_y and B_t generally coincide with the inflection point of B_z bipolar as marked by the vertical dashed lines in both cases.

The amplitude of B_z bipolar from peak to peak is ~ 50 nT for the PFR and ~ 60 nT for the TFR. The enhancements in B_y are ≥ 20 nT and B_t are ≥ 15 nT higher than the ambient field strengths for both cases. To further evaluate the flux ropes, we have applied the minimum (or maximum) variance analysis (MVA) [*Sonnerup and Cahill*, 1967; *Sonnerup and Scheible*, 1998] to the structures and show the result of planetward flux rope in Figure 4c. MVA provides three eigenvalues and three eigenvectors with the ratios between eigenvalues indicating the accuracy of the determined eigenvectors. The eigenvectors help us to understand the orientation of flux ropes with respect to Mercury. The maximum eigenvalues (λ_{max}) for both events are close to the intermediate eigenvalues (λ_{int}, $\lambda_{max}/\lambda_{int} \sim 3$), but are much larger than the minimum eigenvalues (λ_{min}, $\lambda_{int}/\lambda_{min} > 30$), which is the expected result when applying MVA to flux ropes [*Sonnerup and Scheible*, 1998; *Xiao et al*., 2004; *DiBraccio et al*., 2015]. For both events, the maximum variance vectors $(\vec{n}_{max})$ are primarily along the Z'_{MSM} direction, which are consistent with the of B_z bipolar and the minimum variance vectors $(\vec{n}_{min})$ along X'_{MSM} consistent with the observations that B_x is the least perturbed component. The intermediate variance vectors $(\vec{n}_{int})$ are almost in Y'_{MSM} direction showing the axial direction of the flux ropes are mainly along the Y'_{MSM} direction. These MVA results are consistent with the previous observations of flux ropes in both Earth's and Mercury's plasma sheets [e.g., *Slavin et al*., 1993; *Zong et al*., 1997; *DiBraccio et al*., 2015]. In B_{int} versus B_{max} hodograms (Figure 4c), the field rotations (≥180°) further confirm the magnetic field topology of flux ropes.

Traveling compression regions (TCRs) were first observed to be the compressional regions in the lobes caused by the motion of flux ropes in the plasma sheet [*Slavin et al*., 1984, 2005]. At Mercury, the traveling of FTEs along the tail magnetopause was also observed to be accompanied with TCRs in the magnetotail [*Slavin et al*., 2012a]. Figure 5 shows a TCR detected by MESSENGER in the north lobe of Mercury's magnetotail. During this event, B_z is close to zero and B_x (~48 nT) is much larger than the B_z indicating MESSENGER was located in the lobe region, which is further confirmed by FIPS observations (not shown). The TCR exhibits the signatures of increases in B_x

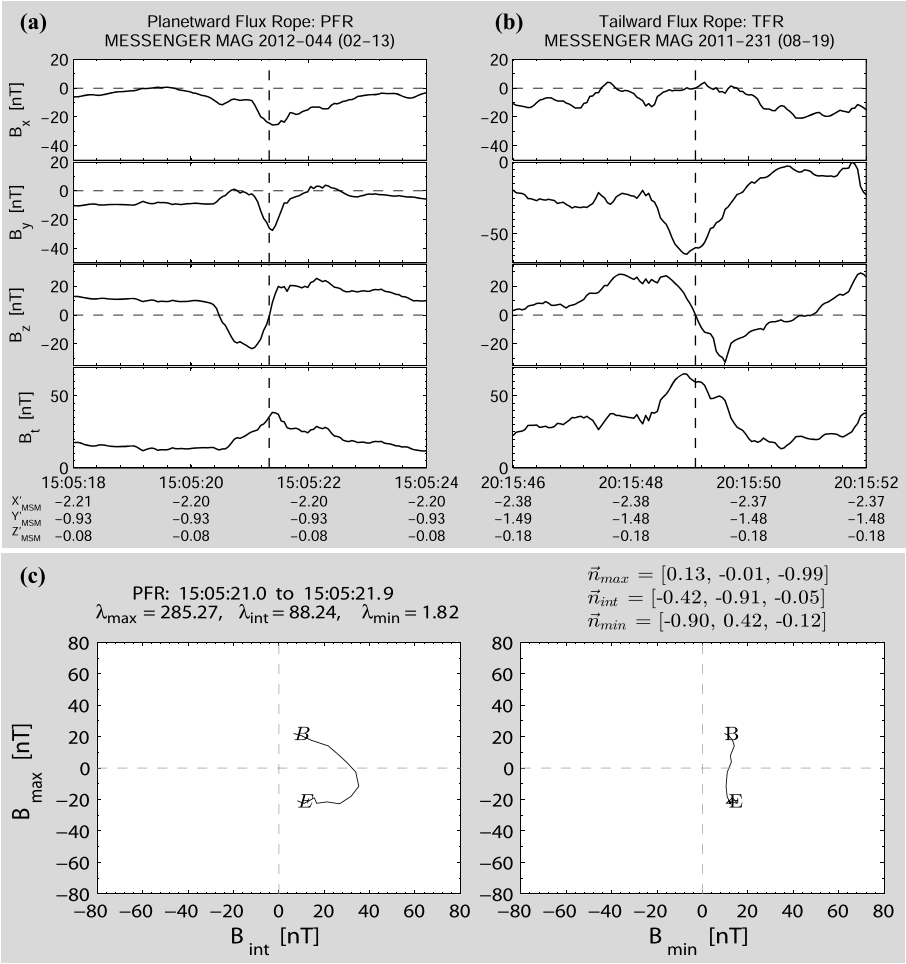

Figure 4. MESSENGER observations of (a) a planetward traveling flux rope (PFR) and (b) a tailward traveling flux rope (TFR). The vertical dashed line marks the inflection point of the B_z bipolar in each column. (c) Hodograms of the magnetic field measurements in MVA coordinates for the PFR.

and B_t together with the highly asymmetric bipolar in B_z (Figure 5a), which are the typical features of TCRs as reported at Earth and Mercury [*Slavin et al*., 2005, 2009, 2012b]. MVA results (Figure 5b) show that the ratios of λ_{max} to λ_{int} and λ_{int} to λ_{min} are ~5 and ~60, respectively, suggesting that the MVA coordinates are well determined. For this TCR, $\vec{n}_{max}$ is mainly along the Z'_{MSM} axis similar to the result of flux rope. But $\vec{n}_{int}$ is along X'_{MSM} and $\vec{n}_{min}$ along Y'_{MSM}, which is opposite to the flux rope with $\vec{n}_{int}$ along Y'_{MSM} and $\vec{n}_{min}$ along X'_{MSM}. This is because TCR consists of the compressed magnetic field lines without helical field topology. In this study, we only consider the flux ropes in the plasma sheet and exclude the TCRs by the above properties.

The survey by *DiBraccio et al*. [2015] have revealed certain values of changes in B_z and B_t (ΔB_z and ΔB_t) for flux ropes in Mercury's magnetotail; i.e., $\Delta B_z \geq 20$ nT and $\Delta B_t \geq 10$ nT. In that study they exclude the events that MESSENGER crossed the outer edge of the flux rope. After surveying many events (~20 events), we have set $\Delta B_z \geq 15$ nT and $\Delta B_t \geq 5$ nT aiming to include more events. The durations for most flux ropes in that work are smaller than 1 s but sometimes could be larger than 3 s [*Slavin et al*., 2012b; *DiBraccio et al*., 2015]. We have applied the following criteria to select flux ropes in this study:

1. Plasma sheet durations are selected based on $\beta_p \geq 0.5$, and the durations under extreme solar wind conditions [*Slavin et al*., 2014] are excluded.
2. Magnetic field data within the plasma sheet are continuously scanned one data point at a time (t_0) with different intervals ($\pm\Delta t$) on either side of that point. We have set three values (i.e., 0.5 s, 1.25 s, and 2.5 s) for Δt.

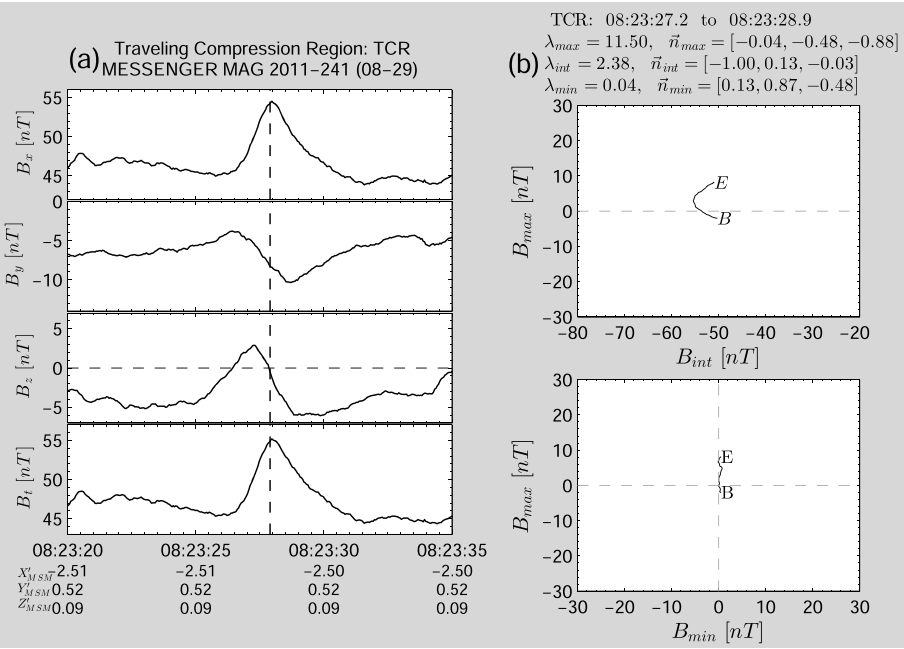

Figure 5. (a) Magnetic field measurement of a tailward traveling compression region (TCR), the vertical dashed line marks the inflection point of B_z bipolar. (b) Hodograms of the magnetic field data in MVA coordinates for the TCR.

3. The minimum B_z (B_{zmin}, corresponding to t_{min}) in the $t_0 - \Delta t$ to $t_0 + \Delta t$ time range should be smaller than 0. The maximum B_z (B_{zmax}, corresponding t_{max}) should be greater than 0, and $B_{zmax} - B_{zmin}$ should be greater than 15 nT. For PFRs, $t_{max} > t_{min}$, while for TFRs, $t_{max} < t_{min}$. We note that TCRs in the plasma sheet generated by magnetopause FTE shower could be avoided by this step as they usually are not accompanied with B_z reversals [*Slavin et al.*, 2012a].
4. The maximum B_y and B_t between t_{min} to t_{max} should be at least 5 nT larger than the average B_y and B_t in the $t_{min} - 0.5$ to t_{min} and t_{max} to $t_{max} + 0.5$ time ranges, individually. TCRs are commonly accompanied with B_x enhancements. This step could further exclude the TCRs in plasma sheet.
5. Applying MVA on the selected events based on criteria (1)–(4) to further pick up the events showing clear magnetic field rotation (angle $\geq 180°$) in the newly formed coordinates.
6. In the newly formed coordinates, B_{max} should show the bipolar signature, and the inflection point coincides with the local maxima in B_{int}.

4.2. Reconnection Fronts Selection

A reconnection front is defined as the leading edge of planetward propagating dipolarizing flux bundle (DFB, also called plasma bubble) [e.g., *Sergeev et al.*, 1996; *Angelopoulos et al.*, 2013; *Sun et al.*, 2014], which is believed to be highly related with magnetic reconnection [e.g., *Sitnov et al.*, 2009; *Ashour-Abdalla et al.*, 2015]. Figure 6a shows a typical DFB detected by MESSENGER in Mercury's plasma sheet, which is defined to be the region between the two vertical dashed lines. The DFB contains stronger magnetic field ($B_t \sim 20$ nT) than the value in ambient plasma sheet ($B_t \sim 8$ nT). The leading edge of this DFB (the first vertical dashed line) is a well-defined reconnection front observed at ~ 21:29:48 UT, which shows a decrease in B_z (called magnetic dip) followed by a sharp increase in B_z (from ~ 5 nT to ~ 25 nT) and B_t (from ~ 8 nT to ~ 27 nT) in ~0.8 s. Application of MVA on the reconnection fronts shows that the ratios of λ_{max} to λ_{int} and λ_{int} to λ_{min} are ~ 180 and ~ 5, respectively, indicating that it is a well-defined one-dimensional structure. Figure 6b shows the magnetic field hodograms under MVA coordinates for the reconnection front. There is no clear field rotation in the hodograms, but the magnetic field perturbation mainly lies in $\vec{n}_{max}$, which further confirms that reconnection front is one-dimensional structure. This agrees with previous observations at Mercury [*Sundberg et al.*, 2012a] and Earth [*Angelopoulos et al.*, 2013; *Liu et al.*, 2013; *Sun et al.*, 2013]. This DFB ends at ~ 21:29:55 UT marked by the second vertical dashed line. This structure lasts ~ 7 s, which is comparable to the duration of DFB in previous

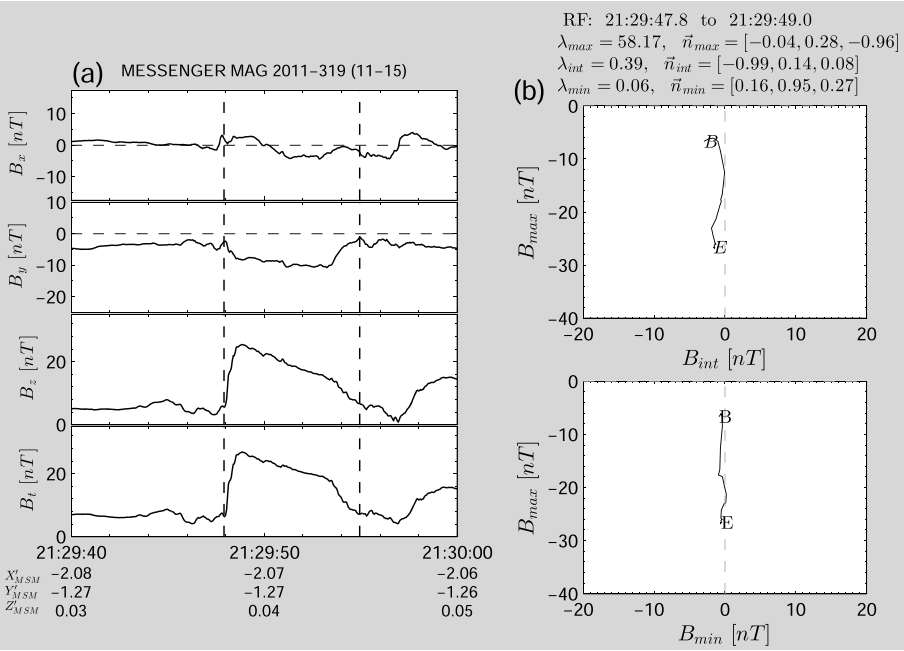

Figure 6. (a) The magnetic field measurements of a dipolarizing flux bundle (DFB, also called plasma bubble) with the leading and trailing edges marked by the two vertical dashed lines. The leading edge is defined as reconnection front (RF, also called dipolarization front). (b) Hodograms of the magnetic field data in MVA coordinates for the reconnection front.

observations (~10 s) at Mercury [*Sundberg et al*., 2012a], but much shorter than the duration of DFBs at Earth (~60 s) [e.g., *Sergeev et al*., 1996; *Sun et al*., 2014].

Another property of DFB is that it contains depleted plasma comparing with ambient plasma sheet [e.g., *Chen and Wolf*, 1993; *Sergeev et al*., 1996; *Sun et al*., 2014]. Since the duration of DFB (~10 s) is normally much shorter than the resolution of plasma moments (1 min), we do not have density measurements within DFB. Therefore, we only employ magnetic field measurements to identify the reconnection fronts in this study. After surveying several tens of reconnection fronts (including those in *Sundberg et al*. [2012a]), we have set up the following criteria to select reconnection fronts:

1. Based on the plasma sheet durations given in section 4.1, magnetic field data inside the plasma sheet are continuously scanned one data point at a time (t_0) with a window of $\pm\Delta t = 1.5$ s on either side of that point, creating an interval of $[t_0 - \Delta t, t_0 + \Delta t]$.
2. The time of maximum B_z ($B_{z\mathrm{max}}$) should be behind the minimum B_z ($B_{z\mathrm{min}}$) in the $t_0 - \Delta t$ to $t_0 + \Delta t$ time range, and $B_{z\mathrm{max}} - B_{z\mathrm{min}}$ should be greater than 15 nT.
3. The averaged B_z (B_t) in the interval $[t_0 + \Delta t, t_0 + \Delta t + 1$ s] should be at least 10 nT (5 nT) greater than in the $[t_0 - \Delta t - 1$ s, $t_0 - \Delta t]$.
4. Exclude the flux ropes listed in section 4.1.

4.3. Statistical Results

The examination of 98 plasma sheet crossings during the three hot seasons obtained 39 flux ropes and 86 reconnection fronts based on the criteria described in sections 4.1 and 4.2. This section shows the statistical results of the flux ropes and reconnection fronts. The histograms in Figure 7 show the distribution of MVA ratios of $\lambda_{max}/\lambda_{int}$ and $\lambda_{int}/\lambda_{min}$ for flux ropes and reconnection fronts. The average values of $\lambda_{max}/\lambda_{int}$ and $\lambda_{int}/\lambda_{min}$ for flux ropes are 5.0 and 17.2, respectively, implying that most of the $\vec{n}_{min}$ are well determined, which is consistent with the results of *DiBraccio et al*. [2015]. The ratios of $\lambda_{max}/\lambda_{int}$ and $\lambda_{int}/\lambda_{min}$ for reconnection fronts have the average values of 32.6 and 13.4, respectively, indicating that the structures are well-defined one-dimensional current sheets. This is also consistent with previous studies [e.g., *Liu et al*., 2013; *Sun et al*., 2013; *Sundberg et al*., 2012a].

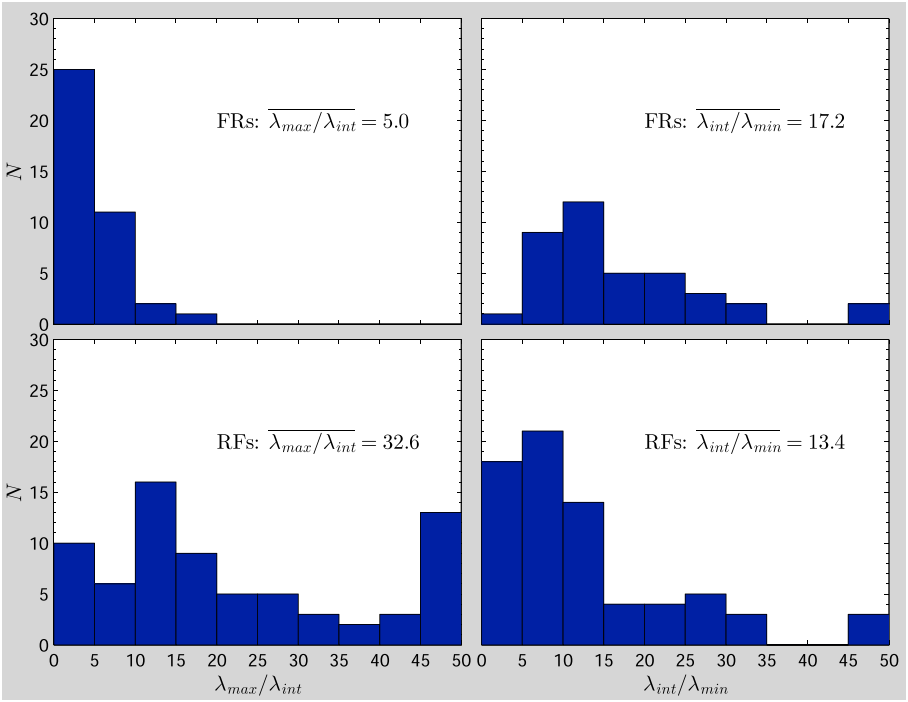

Figure 7. Histograms of the ratio distributions for (top row) FRs and (bottom row) RFs. The ratios of (left column) maximum to intermediate eigenvalues and (right column) intermediate to minimum eigenvalues are shown. The average values of each figure are shown in the middle.

To further confirm the selection of flux ropes, Figure 8 shows the distribution of MVA eigenvectors with flux rope locations. In each case, the $\vec{n}_{max}$ vector is rotated to be positive along the Z'_{MSM}. The $\vec{n}_{int}$ vector is positive along the Y'_{MSM}, and $\vec{n}_{min}$ vector completes the right-handed coordinate system. It can be seen that $\vec{n}_{max}$ is primarily along the Z'_{MSM} direction (Figure 8, left column), $\vec{n}_{int}$ primarily along the Y'_{MSM} direction (Figure 8, middle column), and $\vec{n}_{min}$ primarily along the X'_{MSM} direction (Figure 8, right column), respectively. These $\vec{n}_{int}$ vectors confirm that most of the observed flux ropes have axial directions along Y'_{MSM}. The histograms below each vector projection show the distribution of separation angles between $\vec{n}_{max}$ and Z'_{MSM}, i.e., $\psi\langle\vec{n}_{max},\vec{z}_{MSM}\rangle$; $\vec{n}_{int}$, and Y'_{MSM}, $\psi\langle\vec{n}_{int},\vec{y}_{MSM}\rangle$; and $\vec{n}_{min}$ and X'_{MSM}, and $\psi\langle\vec{n}_{min},\vec{x}_{MSM}\rangle$; respectively. The average values for the separation angles are small (28.1°, 36.3°, and 31.7°) confirming the above conclusions inferred from the distribution of MVA eigenvectors. It can be noticed that several of the $\vec{n}_{int}$ vectors shown in Figure 8 (middle column) appear tilt toward the X'_{MSM}. On the one hand, this would suggest that the axial direction of these flux ropes is skewed in the X'_{MSM}-Y'_{MSM} plane. This phenomenon has been reported in the Earth's magnetotail, which is believed to be due to one end of flux rope is released prior to the release of the other end [e.g., *Moldwin and Hughes*, 1992; *Kiehas et al*., 2012]. On the other hand, this could be due to the deviations in the MVA determined $\vec{n}_{int}$.

Figure 9 shows the distributions of separation angles between MVA eigenvectors of reconnection fronts and the axes of MSM'. We have done the similar rotation for MVA eigenvectors of reconnection fronts as flux ropes. The $\vec{n}_{max}$ for reconnection fronts are mostly aligned with Z'_{MSM} with the average value of $\psi\langle\vec{n}_{max},\vec{z}_{MSM}\rangle$ 26.8°, which is consistent with the most prominent signature of reconnection front, i.e., sharp increase of B_z. But the separation angles between $\vec{n}_{int}$ and Y'_{MSM} and between $\vec{n}_{min}$ and X'_{MSM} are evenly distributed with the average value close to 45°. We suggest that this is due to the shape of reconnection front in the X'_{MSM}-Y'_{MSM} plane being close to a semicircle [e.g., *Pritchett and Coroniti*, 2010; *Liu et al*., 2013; *Sun et al*., 2014], and the reconnection fronts in this study are close to the region of NMNL; i.e., reconnection fronts are "young." Thus, the DFBs should predominately move toward the planet with small Y'_{MSM} and Z'_{MSM} velocity components, which would result MESSENGER crossing any portion of the semicircle reconnection front in equal probability. As a result, the separation angles between the normal of reconnection front $(\vec{n}_{min})$ and X'_{MSM} are evenly distributed in the range of 0° to 90°.

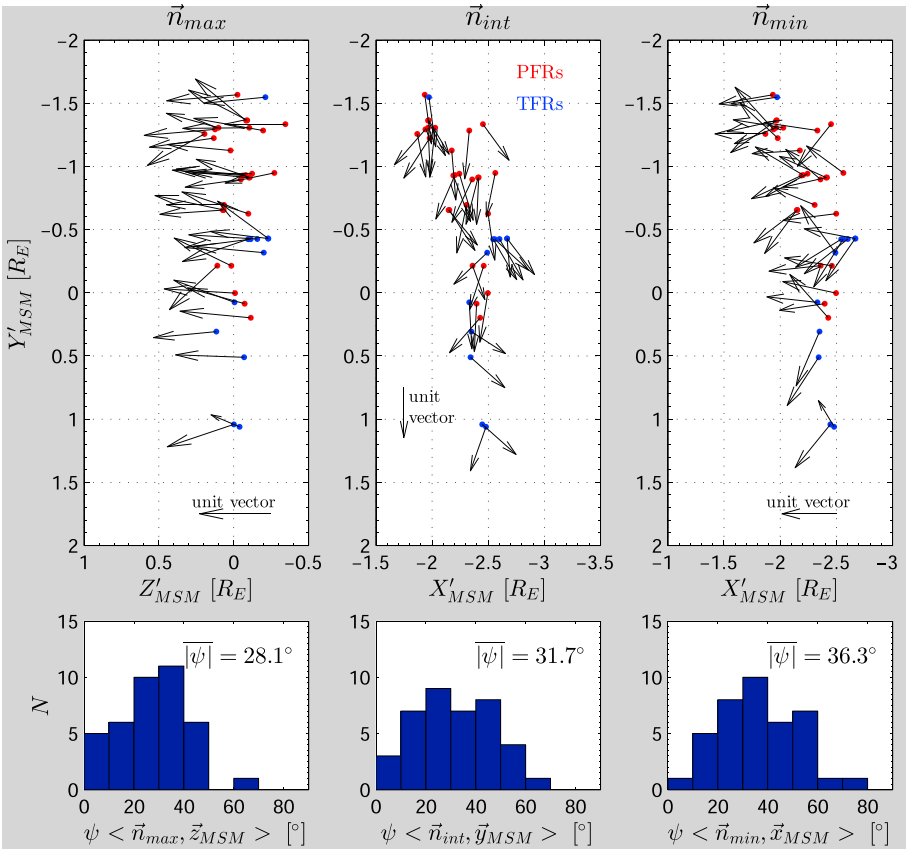

Figure 8. (top row) The projections of $\vec{n}_{max}$ onto the X'_{MSM}-Z'_{MSM} plane, $\vec{n}_{int}$ onto the X'_{MSM}-Y'_{MSM} plane, and $\vec{n}_{min}$ onto the X'_{MSM}-Y'_{MSM} plane, respectively. Red and blue dots represent the locations of PFRs and TFRs. (bottom row) Three histograms from left to right show the separation angles between $\vec{n}_{max}$ and Z'_{MSM} axis, $\vec{n}_{int}$ and Y'_{MSM} axis, and $\vec{n}_{min}$ and X'_{MSM} axis, respectively. The average values for each separation angle are shown in the middle of each figure.

5. Occurrence Rate of Flux Ropes and Reconnection Fronts

The studies in the Earth's tail have shown dawn-dusk asymmetry of near tail reconnection signatures, such as plasma flows, flux ropes, and reconnection fronts, with the structures more frequently observed on the duskside than on the dawnside of the plasma sheet [e.g., *Slavin et al.*, 2005; *Imber et al.*, 2011; *McPherron et al.*, 2011; *Liu et al.*, 2013]. It is suggested that this asymmetry of near tail reconnection occurrences accounts for the substorm auroral onset normally observed on the premidnight (~23 MLT) sector of polar region at Earth [e.g., *Liou et al.*, 2001; *Frey et al.*, 2004]. In this section, we show the occurrence rate of flux ropes and reconnection fronts and its implication on near tail reconnection site in the Mercury's plasma sheet. We also compare the results with the Earth's observations.

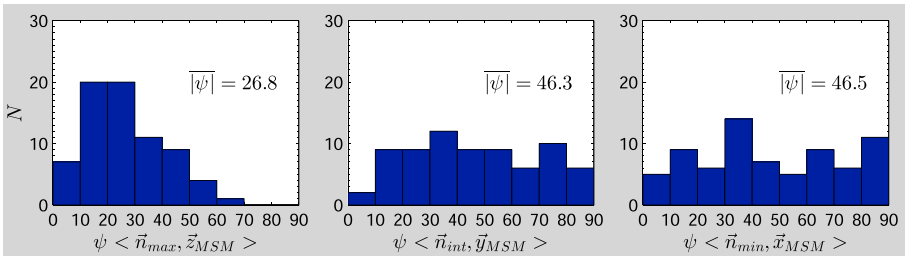

Figure 9. (left, middle, and right) Three histograms of the separation angles between $\vec{n}_{max}$ and Z'_{MSM} axis, $\vec{n}_{int}$ and Y'_{MSM} axis, and $\vec{n}_{min}$ and X'_{MSM} axis, respectively. The average values for each separation angle are shown in the middle of each figure.

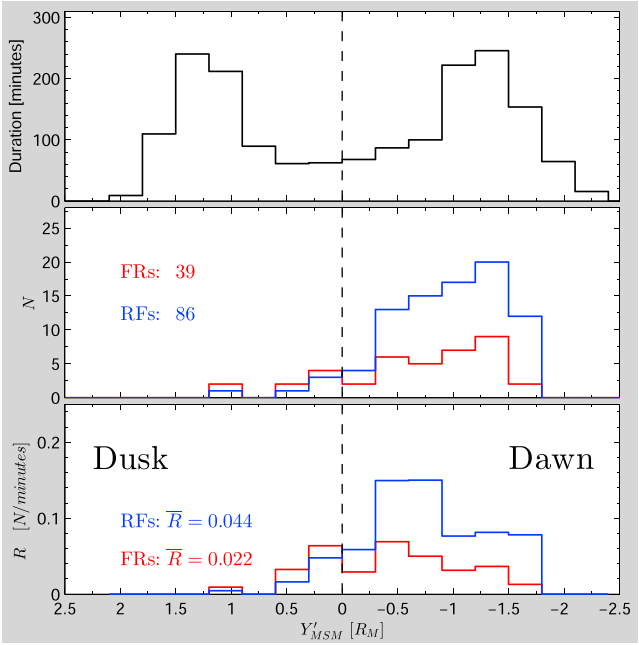

Figure 10. (top, middle, and bottom) The distribution of durations MESSENGER spent in the plasma sheet along Y'_{MSM}, the distribution of number of flux ropes (red line) and reconnection fronts (blue line) along Y'_{MSM}, and the occurrence rates of flux ropes (red line) and reconnection fronts (blue line) along Y'_{MSM}. A dashed line is plotted through $Y'_{MSM} = 0$. The total number of flux ropes and reconnection fronts are shown in the middle panel. The average occurrence rates of flux ropes and reconnection fronts are shown in the bottom panel.

5.1. Dawn-Dusk Distribution

Figure 10 (top) shows the distribution of plasma sheet durations along Y'_{MSM} direction. Plasma sheet is thicker on the dawn and dusk flanks ($|Y'_{MSM}| > 1\,R_M$) than on the midnight region, which will be further discussed in Figure 11. This phenomenon corresponds to the distribution in Figure 10 that MESSENGER spent more time in the dawnside and duskside plasma sheet than in the near-midnight region. Figure 10 (middle) displays the locations of flux ropes (red line, both PFRs and TFRs) and reconnection fronts (blue line). There are obvious asymmetries in these distributions, with more flux ropes and reconnection fronts observed on the dawnside plasma sheet than the duskside plasma sheet. Because the durations MESSENGER stayed in the plasma sheet are not uniform along Y'_{MSM} direction, we have normalized the distribution of flux ropes and reconnection fronts. Figure 10 (bottom) displays the number of events observed per minute along the Y'_{MSM} location. Red line represents the occurrence rates of flux ropes and blue line the reconnection fronts. Both the flux ropes and the reconnection fronts present obvious asymmetries with occurrence rates higher on the dawnside plasma sheet than the duskside plasma sheet. The location of peak occurrence rate for both structures is $\sim Y'_{MSM} = -0.5\,R_M$. The peak occurrence rate of flux ropes is ~ 0.070 events per minute, which is about half of the value (~0.15 events per minute) of reconnection fronts. The average occurrence rate of flux ropes is ~ 0.022 events per minute, which is also half of the occurrence rate of reconnection fronts (~0.044).

5.2. Comparison With Results at Earth

The dawn-dusk asymmetric distributions of the flux ropes and reconnection fronts with events more frequently observed on the dawnside than the duskside plasma sheet at Mercury are different from that at Earth where flux ropes and reconnection fronts more frequently observed on the duskside plasma sheet [*Slavin et al*., 2005; *Imber et al*., 2011; *Liu et al*., 2013]. The dawn-dusk asymmetry of the two structures indicates that the magnetic reconnection is preferentially occurred in the dawnside plasma sheet at Mercury, while the direct observations of ion diffusion region of magnetic reconnection in the Earth's plasma sheet showed more frequently observed on the duskside plasma sheet than on the dawnside plasma sheet [*Nagai et al*., 2013, 2015; *Genestreti et al*., 2014].

In the study of *Liu et al*. [2013], the peak occurrence rate of reconnection fronts is ~ 2.5 events per 1000 min at Earth, i.e., ~ 2.5×10^{-3} events per minute. This value is ~ 60 times smaller than the occurrence rate of reconnection fronts (~0.15 events per minutes) at Mercury shown in this study, and *Imber et al*. [2011] showed that the peak occurrence rate of flux ropes is ~ 0.070 events per hour, i.e., ~ 1.2×10^{-3} events per minute, which is also ~ 60 times smaller than the peak occurrence rate of flux ropes in this study.

A study of flux transfer event (FTE) shower near the magnetopause at Mercury showed the FTE shower had a period of 8 to 10 s [*Slavin et al*., 2012a], which is also ~ 60 times shorter than the quasiperiodic FTEs at Earth with the mean period of ~ 8 min [e.g., *Lockwood and Wild*, 1993]. We note that this difference is

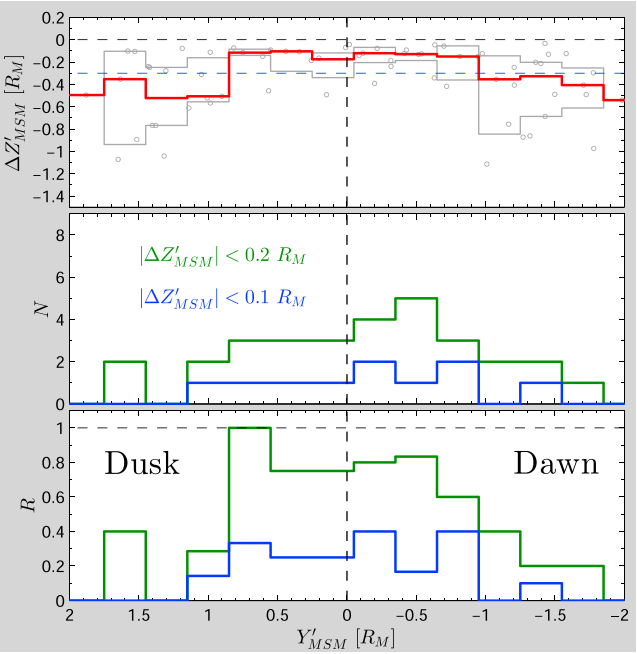

Figure 11. (top) The distribution of plasma sheet thickness. Red line represents the mean value of plasma sheet thickness in each bin, and gray lines represent the upper and lower quartiles. (middle) The distribution of the event number along dawn-dusk direction. Green line represents the events with $|\Delta Z'_{MSM}| < 0.2\ R_M$ and blue line for the events with $|\Delta Z'_{MSM}| < 0.1\ R_M$. (bottom) The occurrence rate for the thin plasma sheet events.

consistent with the differences in occurrence rates for flux ropes and reconnection fronts between Mercury and Earth.

6. Discussion and Conclusions

We interpret the dawn-dusk asymmetric distributions of the flux ropes and reconnection fronts as the reconnection site being preferentially located on the dawnside plasma sheet at Mercury. This is different to the results at Earth showing that reconnection site more frequently occurred on the duskside plasma sheet than on the dawnside [e.g., *Nagai et al.*, 2013, 2015; *Genestreti et al.*, 2014], and there are observations of the clear dawn-dusk asymmetry of the thickness of Earth's plasma sheet with the duskside plasma sheet thinner than the dawnside plasma sheet [e.g., *Fairfield*, 1986; *Rong et al.*, 2011; *Zhang et al.*, 2016]. Therefore, we have estimated the half thickness of plasma sheet in the southern hemisphere for all the plasma sheet crossings based on criteria in section 3.1 to show the distribution of plasma sheet thickness along the Y'_{MSM} locations (Figure 11). We only determine the half thickness of plasma sheet in the southern hemisphere due to the fact that the north boundary of plasma sheet could be affected by the high-latitude plasma sheet when MESSENGER traveled to the northern pole of Mercury.

Each gray circle in Figure 11 (top) represents the half thickness ($\Delta Z'_{MSM}$) of a plasma sheet. The red line is the averaged value of plasma sheet thickness in each bin with the gray lines representing the lower and upper quartiles. Figure 11 (top) shows that plasma sheet near the midnight region ($|Y'_{MSM}| < 0.8\ R_M$) is thinner than the dawn and dusk flank regions ($|Y'_{MSM}| > 0.8\ R_M$). The half thickness of plasma sheet (~0.3 R_M) in the dawn flank region ($Y'_{MSM} < -0.8\ R_M$) is thinner than the value (~0.5 R_M) of dusk flank region ($Y'_{MSM} > 0.8\ R_M$). Magnetic reconnection is believed to occur in thin plasma sheets with thickness comparable or thinner than background proton gyroradius [e.g., *Liu et al.*, 2014a]. Therefore, Figure 11 shows the distribution of plasma sheet with thickness smaller than 0.4 R_M ($|\Delta Z'_{MSM}| < 0.2\ R_M$, green line) and 0.2 R_M ($|\Delta Z'_{MSM}| < 0.1\ R_M$, blue line), respectively. The 0.4 R_M (~980 km) and 0.2 R_M (~490 km) thicknesses of plasma sheet are comparable with the proton gyroradius (~200 to 700 km) for the thin plasma sheet in Figure 2. It can be seen that most of the thin plasma sheets are in the near midnight region ($|Y'_{MSM}| < 0.8\ R_M$), which is confirmed by the distribution of occurrence rate of the thin plasma sheet. There is not an obvious dawn-dusk asymmetry. Thus, it seems that the distribution of thin plasma sheet cannot explain the dawn-dusk asymmetric distributions of flux ropes and reconnection fronts in Mercury's plasma sheet. Research at Earth has shown that the thickness of plasma sheet could differ a lot between the southward and northward IMF periods [*Zhang et al.*, 2016]. Since it is a primary study of plasma sheet thickness distribution in this paper, a further extensive research on the plasma sheet thickness distribution in Mercury's magnetotail is needed.

It should be noted that the heavy ions (Sodium, Na+, and Oxygen, O+) have shown dawn-dusk asymmetry with them enhanced on the duskside plasma sheet in Mercury's magnetotail [*Zurbuchen et al.*, 2011; *Raines et al.*, 2013; *Gershman et al.*, 2014]. But the influence of heavy ions on the initiation of magnetic reconnection

is still in debate. The temperature of sodium in Mercury's plasma sheet was investigated to be similar as proton [*Gershman et al*., 2014]. Thus, the sodium gyroradius would be ~ 23 times larger than proton with a scale of several (~2 to 5) R_M, which is always larger than the thickness of plasma sheet as shown in Figure 11. But the study in the Earth's plasma sheet shows that heavy ions (O+) seems to not affect the scale of reconnecting current sheet even with a high O+ content ($n_{O+}/n_{H+} > 0.083$) [*Liu et al*., 2014b]. Some studies had shown that outflow of O+ from the Earth's ionosphere could increase the occurrence of reconnection in the duskside plasma sheet and therefore facilitate the occurrence of substorm [*Baker et al*., 1982, 1985], while others indicated that higher O+/H+ ratio would suppress substorm occurrence [*Nosé et al*., 2009]. Hence, whether the dawn-dusk asymmetry of magnetic reconnection in Mercury's plasma sheet is due to the influence of heavy ions remains unanswered. It has also been shown that the Kelvin-Helmholtz waves at Mercury are predominately observed on the duskside magnetopause but is seldomly observed on the dawnside magnetopause [*Sundberg et al*., 2012b; *Liljeblad et al*., 2014; *Gershman et al*., 2015]. Because the scale of KH waves at Mercury could be ~ 1 R_M [*Boardsen et al*., 2010], therefore, there will be more solar wind plasma entry on the duskside plasma sheet than on the dawnside. The influence of solar wind plasma on the occurrence of magnetic reconnection at Mercury needs further study.

It has been shown that there is no conducting ionosphere at Mercury. The Region 1 field-aligned currents (FACs) might close through the regolith near Mercury's surface, which is quite distinct from the Earth [*Anderson et al*., 2014]. The magnitude of Region 1 FACs at Mercury (tens of kA) is observed to be 2 orders smaller than that of Earth (several MA). But the strength varies with different disturbance levels [*Anderson et al*., 2014], similar to the result at Earth [*Alexeev et al*., 2000]. No Region 2 FAC signature was detected at Mercury. Mercury's magnetosphere is also different to the Earth's in many other aspects, such as the scale of Mercury's magnetosphere is much smaller [e.g., *Ness et al*., 1974; *Alexeev et al*., 2008], the relative polar cap size of Mercury is larger [*Alexeev et al*., 2008], and the relatively loaded magnetic flux during magnetospheric substorm is larger [*Slavin et al*., 2010b; *Sun et al*., 2015a]. How these differences influence the dynamics of Mercury's magnetosphere desire for further study.

The study from Earth showed close relation between plasmoids (and high-speed flows) in the tail with auroral brightening in the polar region [e.g., *Fairfield et al*., 1999; *Ieda et al*., 2001], and the premidnight onset location of Earth's substorm agrees with the average location of reconnection site in the magnetotail [e.g., *Imber et al*., 2011]. The higher occurrence of flux ropes and reconnection fronts in the dawnside plasma sheet indicates that magnetic reconnection more frequently occurred in the dawnside plasma sheet and, therefore, generate more plasma flows in the dawnside plasma sheet at Mercury. Thus, it would be expected that more fast flows brake and initiate substorm onset on the postmidnight sector at Mercury, which is different from the well determined premidnight onset locations of substorm at Earth [e.g., *Liou et al*., 2001; *Frey et al*., 2004]. Energetic electrons in Mercury's magnetosphere are more frequently detected on the premidnight sector than on the postmidnight sector [*Lawrence et al*., 2015; *Baker et al*., 2016; *Ho et al*., 2016; *Lindsay et al*., 2016]. This is commonly believed to be due to the dawnward drift of electrons in the magnetosphere of Mercury. Our observations would indicate that this could also be due to more flow bursts brake on the postmidnight sector than on the premidnight sector at Mercury. The substorm dipolarizations during flow brake would energize the electrons and result in more energetic electrons on the postmidnight sector. This process is schematically shown in Figure 12.

The occurrence rate of flux ropes and reconnection fronts in Mercury's magnetotail is ~ 60 times higher than the observations in Earth's magnetotail, which indicates that the occurrence rate of magnetic reconnection in the Mercury's plasma sheet is much higher than the Earth's plasma sheet. Considering that the ~ 2 to 3 min magnetic flux circulation time at Mercury, i.e., Dungey circulation or magnetospheric substorm [*Slavin et al*., 2010b; *Sun et al*., 2015b], is also ~ 60 times shorter than the duration (~2 to 3 h) at Earth [e.g., *Akasofu*, 1964; *Baker et al*., 1996], we conclude that the higher occurrence rate of magnetic reconnection at Mercury is due to its highly variable magnetospheric dynamics.

This study of flux ropes and reconnection fronts in Mercury's magnetotail and comparison with Earth's results have revealed a number of important features for Mercury's magnetosphere.

1. The distribution of flux ropes and reconnection fronts shows a clear dawn-dusk asymmetry with higher occurrence rate on the dawnside than on the duskside in region of NMNL, which suggests that the magnetic reconnection occurs more frequently on the dawnside than on the duskside in Mercury's magnetotail. This is

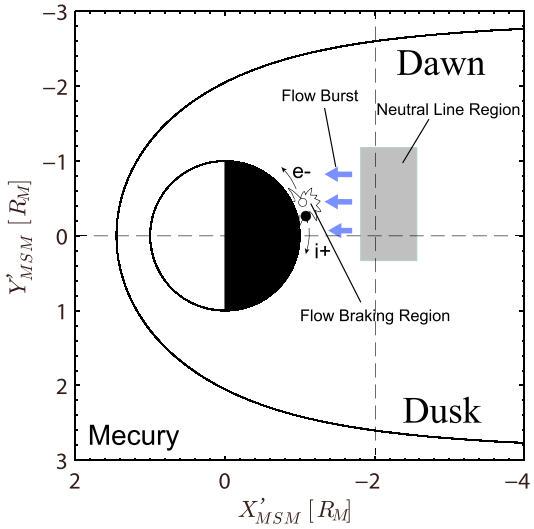

Figure 12. Schematic view of reconnection locations and flow braking region at Mercury. Gray region indicate the detected near-tail neutral line regions for both planets. Blue arrows represent reconnection generated planetward propagating flow bursts.

different to the observations in Earth's magnetotail showing more reconnection on the duskside plasma sheet.

2. The peak occurrence rates of flux ropes and reconnection fronts in Mercury's plasma sheet are ~60 times higher than that of Earth's. This could be due to highly variable magnetospheric conditions at Mercury with the time scale of global flux circulation the similar value faster than the Earth.

Furthermore, the results indicate that higher occurrence rate of magnetic reconnection would generate more flow bursts in the dawnside plasma sheet than in the duskside. As a result, flow bursts would mostly brake and initiate the substorm on the postmidnight sector at Mercury rather than the premidnight substorm onset location at Earth. We propose the observations of energetic electrons showing that more events in the postmidnight sector than premidnight sector could be due to not only the dawnward drift of electrons but also the postmidnight substorm initiation (i.e., substorm dipolarizations).

Acknowledgments

The data used in this study were available from the Planetary Data System (PDS): http://pds.jpl.nasa.gov. The MESSENGER project is supported by the NASA Discovery Program under contracts NASW-00002 to the Carnegie Institution of Washington and NAS5-97271 to The Johns Hopkins University Applied Physics Laboratory. Wei-Jie Sun is supported by the State Scholarship Fund of Chinese Scholarship Council. This work is supported by the National Nature Science Foundation of China (grants 41474139 and 41421003). This work is also supported by the NASA Heliophysics Supporting Research Program under grant NNX15AJ68G. Wei-Jie Sun thanks Xu-Zhi Zhou (Peking University, China) for helpful discussion.

References

Akasofu, S. I. (1964), The development of the auroral substorm, *Planet. Space Sci.*, *12*(4), 273–282, doi:10.1016/0032-0633(64)90151-5.

Alexeev, I. I., E. S. Belenkaya, and C. R. Clauer Jr. (2000), A model of region 1 field-aligned currents dependent on ionospheric conductivity and solar wind parameters, *J. Geophys. Res.*, *105*, 21,119–21,127, doi:10.1029/2000JA900052.

Alexeev, I. I., E. S. Belenkaya, S. Yu. Bobrovnikov, J. A. Slavin, and M. Sarantos (2008), Paraboloid model of Mercury's magnetosphere, *J. Geophys. Res.*, *113*, A12210, doi:10.1029/2008JA013368.

Alexeev, I. I., et al. (2010), Mercury's magnetospheric magnetic field after the first two MESSENGER flybys, *Icarus*, *209*(1), 23–39, doi:10.1016/j.icarus.2010.01.024.

Anderson, B. J., M. H. Acuña, D. A. Lohr, J. Scheifele, A. Raval, H. Korth, and J. A. Slavin (2007), The magnetometer instrument on MESSENGER, *Space Sci. Rev.*, *131*(1-4), 417–450, doi:10.1007/s11214-007-9246-7.

Anderson, B. J., et al. (2010), The magnetic field of Mercury, *Space Sci. Rev.*, *152*(1-4), 307–339, doi:10.1007/s11214-009-9544-3.

Anderson, B. J., C. L. Johnson, H. Korth, M. E. Purucker, R. M. Winslow, J. A. Slavin, S. C. Solomon, R. L. McNutt Jr., J. M. Raines, and T. H. Zurbuchen (2011), The global magnetic field of Mercury from MESSENGER orbital observations, *Science*, *333*(6051), 1859–1862, doi:10.1126/science.1211001.

Anderson, B. J., C. L. Johnson, H. Korth, J. A. Slavin, R. M. Winslow, R. J. Phillips, R. L. McNutt Jr., and S. C. Solomon (2014), Steady-state field-aligned currents at Mercury, *Geophys. Res. Lett.*, *41*, 7444–7452, doi:10.1002/2014GL061677.

Andrews, G. B., et al. (2007), The energetic particle and plasma spectrometer instrument on the MESSENGER spacecraft, *Space Sci. Rev.*, *131*(1-4), 523–556, doi:10.1007/s11214-007-9272-5.

Angelopoulos, V., C. F. Kennel, F. V. Coroniti, R. Pellat, M. G. Kivelson, R. J. Walker, C. T. Russell, W. Baumjohann, W. C. Feldman, and J. T. Gosling (1994), Statistical characteristics of bursty bulk flow events, *J. Geophys. Res.*, *99*, 21,257–21,280, doi:10.1029/94JA01263.

Angelopoulos, V., A. Runov, X.-Z. Zhou, D. L. Turner, S. A. Kiehas, S.-S. Li, and I. Shinohara (2013), Electromagnetic energy conversion at reconnection fronts, *Science*, *341*(6153), 1478–1482, doi:10.1126/science.1236992.

Ashour-Abdalla, M., G. Lapenta, R. J. Walker, M. El-Alaoui, and H. Liang (2015), Multiscale study of electron energization during unsteady reconnection events, *J. Geophys. Res. Space Physics*, *120*, 4784–4799, doi:10.1002/2014JA020316.

Baker, D. N., E. W. Hones, D. T. Young, and J. Birn (1982), The possible role of ionospheric oxygen in the initiation and development of plasma sheet instabilities, *Geophys. Res. Lett.*, *9*, 1337–1340, doi:10.1029/GL009i012p01337.

Baker, D. N., T. A. Fritz, W. Lennartsson, B. Wilken, H. W. Kroehl, and J. Birn (1985), The role of heavy ionospheric ions in the localization of substorm disturbances on March 22, 1979: CDAW 6, *J. Geophys. Res.*, *90*, 1273–1281, doi:10.1029/JA090iA02p01273.

Baker, D. N., T. I. Pulkkinen, V. Angelopoulos, W. Baumjohann, and R. L. McPherron (1996), Neutral line model of substorms: Past results and present view, *J. Geophys. Res.*, *101*, 12,975–13,010, doi:10.1029/95JA03753.

Baker, D. N., et al. (2016), Intense energetic electron flux enhancements in Mercury's magnetosphere: An integrated view with high-resolution observations from MESSENGER, *J. Geophys. Res. Space Physics*, *121*, 2171–2184, doi:10.1002/2015JA021778.

Baumjohann, W., G. Paschmann, and C. A. Cattell (1989), Average plasma properties in the central plasma sheet, *J. Geophys. Res.*, *94*, 6597–6606, doi:10.1029/JA094iA06p06597.

Baumjohann, W., G. Paschmann, and H. Lühr (1990), Characteristics of high-speed ion flows in the plasma sheet, *J. Geophys. Res.*, *95*, 3801–3809, doi:10.1029/JA095iA04p03801.

Boardsen, S. A., T. Sundberg, J. A. Slavin, B. J. Anderson, H. Korth, S. C. Solomon, and L. G. Blomberg (2010), Observations of Kelvin-Helmholtz waves along the dusk-side boundary of Mercury's magnetosphere during MESSENGER's third flyby, *Geophys. Res. Lett.*, *37*, L12101, doi:10.1029/2010GL043606.

Chen, C. X., and R. A. Wolf (1993), Interpretation of high-speed flows in the plasma sheet, *J. Geophys. Res.*, *98*, 21,409–21,419, doi:10.1029/93JA02080.

Cowley, S. W. H. (1981), Magnetospheric asymmetries associated with the *y*-component of the IMF, *Planet. Space Sci.*, *29*(1), 79–96, doi:10.1016/0032-0633(81)90141-0.

DiBraccio, G. A., et al. (2015), MESSENGER observations of flux ropes in Mercury's magnetotail, *Planet. Space Sci.*, *115*, 77–89, doi:10.1016/j.pss.2014.12.016.

Fairfield, D. H. (1986), The magnetic field of the equatorial magnetotail from 10 to 40 R_E, *J. Geophys. Res.*, *91*, 4238–4244, doi:10.1029/JA091iA04p04238.

Fairfield, D. H., et al. (1999), Earthward flow bursts in the inner magnetotail and their relation to auroral brightenings, AKR intensifications, geosynchronous particle injections and magnetic activity, *J. Geophys. Res.*, *104*, 355–370, doi:10.1029/98JA02661.

Frey, H. U., S. B. Mende, V. Angelopoulos, and E. F. Donovan (2004), Substorm onset observations by IMAGE-FUV, *J. Geophys. Res.*, *109*, A10304, doi:10.1029/2004JA010607.

Fu, H. S., et al. (2013), Dipolarization fronts as a consequence of transient reconnection: In situ evidence, *Geophys. Res. Lett.*, *40*, 6023–6027, doi:10.1002/2013GL058620.

Genestreti, K. J., S. A. Fuselier, J. Goldstein, T. Nagai, and J. P. Eastwood (2014), The location and rate of occurrence of near-Earth magnetotail reconnection as observed by Cluster and Geotail, *J. Atmos. Sol. Terr. Phys.*, *121*(Part A), 98–109, doi:10.1016/j.jastp.2014.10.005.

Gershman, D. J., J. A. Slavin, J. M. Raines, T. H. Zurbuchen, B. J. Anderson, H. Korth, D. N. Baker, and S. C. Solomon (2013), Magnetic flux pileup and plasma depletion in Mercury's subsolar magnetosheath, *J. Geophys. Res. Space Physics*, *118*, 7181–7199, doi:10.1002/2013JA019244.

Gershman, D. J., et al. (2014), Ion kinetic properties in Mercury's pre-midnight plasma sheet, *Geophys. Res. Lett.*, *41*, 5740–5747, doi:10.1002/2014GL060468.

Gershman, D. J., J. M. Raines, J. A. Slavin, T. H. Zurbuchen, T. Sundberg, S. A. Boardsen, B. J. Anderson, H. Korth, and S. C. Solomon (2015), MESSENGER observations of multiscale Kelvin-Helmholtz vortices at Mercury, *J. Geophys. Res. Space Physics*, *120*, 4354–4368, doi:10.1002/2014JA020903.

Glassmeier, K. (1997), The Hermean magnetosphere and its ionosphere-magnetosphere coupling, *Planet. Space Sci.*, *45*(1), 119–125, doi:10.1016/S0032-0633(96)00095-5.

Ho, G. C., et al. (2016), MESSENGER observations of suprathermal electrons in Mercury's magnetosphere, *Geophys. Res. Lett.*, *43*, 550–555, doi:10.1002/2015GL066850.

Hones, E. W. (1977), Substorm processes in the magnetotail: Comments on "On hot tenuous plasmas, fireballs, and boundary layers in the Earth's magnetotail" by L. A. Frank, K. L. Ackerson, and R. P. Lepping, *J. Geophys. Res.*, *82*, 5633–5640, doi:10.1029/JA082i035p05633.

Hughes, W. J., and D. G. Sibeck (1987), On the 3-dimensional structure of plasmoid, *Geophys. Res. Lett.*, *14*, 636–639, doi:10.1029/GL014i006p00636.

Ieda, A., D. H. Fairfield, T. Mukai, Y. Saito, S. Kokubun, K. Liou, C.-I. Meng, G. K. Parks, and M. J. Brittnacher (2001), Plasmoid ejection and auroral brightenings, *J. Geophys. Res.*, *106*, 3845–3857, doi:10.1029/1999JA000451.

Imber, S. M., J. A. Slavin, H. U. Auster, and V. Angelopoulos (2011), A THEMIS survey of flux ropes and traveling compression regions: Location of the near-Earth reconnection site during solar minimum, *J. Geophys. Res.*, *116*, A02201, doi:10.1029/2010JA016026.

Johnson, C. L., et al. (2012), MESSENGER observations of Mercury's magnetic field structure, *J. Geophys. Res.*, *117*, E00L14, doi:10.1029/2012JE004217.

Kiehas, S. A., V. Angelopoulos, A. Runov, M. B. Moldwin, and C. Möstl (2012), On the formation of tilted flux ropes in the Earth's magnetotail observed with ARTEMIS, *J. Geophys. Res.*, *117*, A05231, doi:10.1029/2011JA017377.

Lawrence, D. J., et al. (2015), Comprehensive survey of energetic electron events in Mercury's magnetosphere with data from the MESSENGER Gamma-Ray and Neutron Spectrometer, *J. Geophys. Res. Space Physics*, *120*, 2851–2876, doi:10.1002/2014JA020792.

Lepping, R. P., D. H. Fairfield, J. Jones, L. A. Frank, W. R. Paterson, S. Kokubun, and T. Yamamoto (1995), Cross-tail magnetic flux ropes as observed by the GEOTAIL spacecraft, *Geophys. Res. Lett.*, *22*, 1193–1196, doi:10.1029/94GL01114.

Liljeblad, E., T. Sundberg, T. Karlsson, and A. Kullen (2014), Statistical investigation of Kelvin-Helmholtz waves at the magnetopause of Mercury, *J. Geophys. Res. Space Physics*, *119*, 9670–9683, doi:10.1002/2014JA020614.

Lindsay, S. T., M. K. James, E. J. Bunce, S. M. Imber, A. Martindale, and T. K. Yeoman (2016), MESSENGER X-ray observations of magnetosphere–surface interaction on the nightside of Mercury, *Planet. Space Sci.*, *125*, 72–79, doi:10.1016/j/pss.2016.03.005.

Liou, K., P. T. Newell, D. G. Sibeck, C.-I. Meng, M. Brittnacher, and G. Parks (2001), Observation of IMF and seasonal effects in the location of auroral substorm onset, *J. Geophys. Res.*, *106*, 5799–5810, doi:10.1029/2000JA003001.

Liu, J., V. Angelopoulos, A. Runov, and X.-Z. Zhou (2013), On the current sheets surrounding dipolarizing flux bundles in the magnetotail: The case for wedgelets, *J. Geophys. Res. Space Physics*, *118*, 2000–2020, doi:10.1002/jgra.50092.

Liu, Y. H., L. M. Kistler, C. G. Mouikis, V. Roytershteyn, and H. Karimabadi (2014b), The scale of the magnetotail reconnecting current sheet in the presence of O+, *Geophys. Res. Lett.*, *41*, 4819–4827, doi:10.1002/2014GL060440.

Liu, Y., J. Birn, W. Daughton, M. Hesse, and K. Schindler (2014a), Onset of reconnection in the near magnetotail: PIC simulations, *J. Geophys. Res. Space Physics*, *119*, 9773–9789, doi:10.1002/2014JA020492.

Lockwood, M., and M. N. Wild (1993), On the quasi-periodic nature of magnetopause flux transfer events, *J. Geophys. Res.*, *98*(A4), 5935–5940, doi:10.1029/92JA02375.

McPherron, R. L., T.-S. Hsu, J. Kissinger, X. Chu, and V. Angelopoulos (2011), Characteristics of plasma flows at the inner edge of the plasma sheet, *J. Geophys. Res.*, *116*, A00I33, doi:10.1029/2010JA015923.

Moldwin, M. B., and W. J. Hughes (1991), Plasmoids as magnetic flux ropes, *J. Geophys. Res.*, *96*(A8), 14,051–14,064, doi:10.1029/91JA01167.

Moldwin, M. B., and W. J. Hughes (1992), On the formation and evolution of plasmoids: A survey of ISEE 3 geotail data, *J. Geophys. Res.*, *97*(A12), 19,259–19,282, doi:10.1029/92JA01598.

Moldwin, M. B., and W. J. Hughes (1994), Observations of earthward and tailward propagating flux rope plasmoids: Expanding the plasmoid model of geomagnetic substorms, *J. Geophys. Res.*, *99*(A1), 183–198, doi:10.1029/93JA02102.

Nagai, T., I. Shinohara, S. Zenitani, R. Nakamura, T. K. M. Nakamura, M. Fujimoto, Y. Saito, and T. Mukai (2013), Three-dimensional structure of magnetic reconnection in the magnetotail from Geotail observations, *J. Geophys. Res. Space Physics*, *118*, 1667–1678, doi:10.1002/jgra.50247.

Nagai, T., I. Shinohara, and S. Zenitani (2015), The dawn-dusk length of the X line in the near-Earth magnetotail: Geotail survey in 1994–2014, *J. Geophys. Res. Space Physics*, *120*, 8762–8773, doi:10.1002/2015JA021606.
Ness, N. F., K. W. Behannon, R. P. Lepping, Y. C. Whang, and K. H. Schatten (1974), Magnetic field observations near Mercury: Preliminary results from Mariner 10, *Science*, *185*(4146), 151–160, doi:10.1126/science.185.4146.151.
Nosé, M., A. Ieda, and S. P. Christon (2009), Geotail observations of plasma sheet ion composition over 16 years: On variations of average plasma ion mass and O+ triggering substorm model, *J. Geophys. Res.*, *114*, A07223, doi:10.1029/2009JA014203.
Pritchett, P. L., and F. V. Coroniti (2010), A kinetic ballooning/interchange instability in the magnetotail, *J. Geophys. Res.*, *115*, A6301, doi:10.1029/2009JA014752.
Raines, J. M., J. A. Slavin, T. H. Zurbuchen, G. Gloeckler, B. J. Anderson, H. Korth, and S. M. Krimigis (2011), MESSENGER observations of the plasma environment near Mercury, *Planet. Space Sci.*, *59*(15), 2004–2015, doi:10.1016/j.pss.2011.02.004.
Raines, J. M., et al. (2013), Distribution and compositional variations of plasma ions in Mercury's space environment: The first three Mercury years of MESSENGER observations, *J. Geophys. Res. Space Physics*, *118*, 1604–1619, doi:10.1029/2012JA018073.
Raj, A., T. Phan, R. P. Lin, and V. Angelopoulos (2002), Wind survey of high-speed bulk flows and field-aligned beams in the near-Earth plasma sheet, *J. Geophys. Res.*, *107*(A12), 1419, doi:10.1029/2001JA007547.
Rong, Z. J., W. X. Wan, C. Shen, X. Li, M. W. Dunlop, A. A. Petrukovich, T. L. Zhang, and E. Lucek (2011), Statistical survey on the magnetic structure in magnetotail current sheets, *J. Geophys. Res.*, *116*, A09218, doi:10.1029/2011JA016489.
Runov, A., V. Angelopoulos, M. I. Sitnov, V. A. Sergeev, J. Bonnell, J. P. McFadden, D. Larson, K.-H. Glassmeier, and U. Auster (2009), THEMIS observations of an earthward-propagating dipolarization front, *Geophys. Res. Lett.*, *36*, L14106, doi:10.1029/2009GL038980.
Russell, C. T., and R. J. Walker (1985), Flux transfer events at Mercury, *J. Geophys. Res.*, *90*(A11), 11,067–11,074, doi:10.1029/JA090iA11p11067.
Sergeev, V. A., V. Angelopoulos, J. T. Gosling, C. A. Cattell, and C. T. Russell (1996), Detection of localized, plasma-depleted flux tubes or bubbles in the midtail plasma sheet, *J. Geophys. Res.*, *101*(A5), 10,817–10,826, doi:10.1029/96JA00460.
Sitnov, M. I., M. Swisdak, and A. V. Divin (2009), Dipolarization fronts as a signature of transient reconnection in the magnetotail, *J. Geophys. Res.*, *114*, A04202, doi:10.1029/2008JA013980.
Slavin, J. A., E. J. Smith, B. T. Tsurutani, D. G. Sibeck, H. J. Singer, D. N. Baker, J. T. Gosling, E. W. Hones, and F. L. Scarf (1984), Substorm associated traveling compression regions in the distant tail: Isee-3 Geotail observations, *Geophys. Res. Lett.*, *11*(7), 657–660, doi:10.1029/GL011i007p00657.
Slavin, J. A., M. F. Smith, E. L. Mazur, D. N. Baker, E. W. Hones Jr., T. Iyemori, and E. W. Greenstadt (1993), ISEE 3 observations of traveling compression regions in the Earth's magnetotail, *J. Geophys. Res.*, *98*(A9), 15,425–15,446, doi:10.1029/93JA01467.
Slavin, J. A., R. P. Lepping, J. Gjerloev, D. H. Fairfield, M. Hesse, C. J. Owen, M. B. Moldwin, T. Nagai, A. Ieda, and T. Mukai (2003), Geotail observations of magnetic flux ropes in the plasma sheet, *J. Geophys. Res.*, *108*(A1), 1015, doi:10.1029/2002JA009557.
Slavin, J. A., E. I. Tanskanen, M. Hesse, C. J. Owen, M. W. Dunlop, S. Imber, E. A. Lucek, A. Balogh, and K.-H. Glassmeier (2005), Cluster observations of traveling compression regions in the near-tail, *J. Geophys. Res.*, *110*, A06207, doi:10.1029/2004JA010878.
Slavin, J. A., et al. (2009), MESSENGER observations of magnetic reconnection in Mercury's magnetosphere, *Science*, *324*(5927), 606–610, doi:10.1126/science.1172011.
Slavin, J. A., et al. (2010a), MESSENGER observations of large flux transfer events at Mercury, *Geophys. Res. Lett.*, *37*, L2105, doi:10.1029/2009GL041485.
Slavin, J. A., et al. (2010b), MESSENGER observations of extreme loading and unloading of Mercury's magnetic tail, *Science*, *329*(5992), 665–668, doi:10.1126/science.1188067.
Slavin, J. A., et al. (2012a), MESSENGER observations of a flux-transfer-event shower at Mercury, *J. Geophys. Res.*, *117*, A00M06, doi:10.1029/2012JA017926.
Slavin, J. A., et al. (2012b), MESSENGER and Mariner 10 flyby observations of magnetotail structure and dynamics at Mercury, *J. Geophys. Res.*, *117*, A01215, doi:10.1029/2011JA016900.
Slavin, J. A., et al. (2014), MESSENGER observations of Mercury's dayside magnetosphere under extreme solar wind conditions, *J. Geophys. Res. Space Physics*, *119*, 8087–8116, doi:10.1002/2014JA020319.
Solomon, S., R. L. McNutt Jr., R. E. Gold, and D. L. Domingue (2007), MESSENGER mission overview, *Space Sci. Rev.*, *131*(1-4), 3–39, doi:10.1007/s11214-007-9247-6.
Sonnerup, B., and M. Scheible (1998), Minimum and maximum variance analysis, in *Analysis Methods for Multi-Spacecraft Data*, edited by G. Paschmann and P. W. Daly, pp. 185–220, ESA Publ, Noordwijk, Netherlands.
Sonnerup, B. U., and L. J. Cahill (1967), Magnetopause structure and attitude from EXPLORER 12 observations, *J. Geophys. Res.*, *72*(1), 171–183, doi:10.1029/JZ072i001p00171.
Sun, W. J., S. Y. Fu, G. K. Parks, J. Liu, Z. H. Yao, Q. Q. Shi, Q.-G. Zong, S. Y. Huang, Z. Y. Pu, and T. Xiao (2013), Field-aligned currents associated with dipolarization fronts, *Geophys. Res. Lett.*, *40*, 4503–4508, doi:10.1002/grl.50902.
Sun, W., S. Fu, Z. Pu, G. K. Parks, J. A. Slavin, Z. Yao, Q.-G. Zong, Q. Shi, D. Zhao, and Y. Cui (2014), The current system associated with the boundary of plasma bubbles, *Geophys. Res. Lett.*, *41*, 8169–8175, doi:10.1002/2014GL062171.
Sun, W., et al. (2015a), MESSENGER observations of Alfvénic and compressional waves during Mercury's substorms, *Geophys. Res. Lett.*, *42*, 6189–6198, doi:10.1002/2015GL065452.
Sun, W., et al. (2015b), MESSENGER observations of magnetospheric substorm activity in Mercury's near magnetotail, *Geophys. Res. Lett.*, *42*, 3692–3699, doi:10.1002/2015GL064052.
Sundberg, T., et al. (2012a), MESSENGER observations of dipolarization events in Mercury's magnetotail, *J. Geophys. Res.*, *117*, A00M03, doi:10.1029/2012JA017756.
Sundberg, T., S. A. Boardsen, J. A. Slavin, B. J. Anderson, H. Korth, T. H. Zurbuchen, J. M. Raines, and S. C. Solomon (2012b), MESSENGER orbital observations of large-amplitude Kelvin-Helmholtz waves at Mercury's magnetopause, *J. Geophys. Res.*, *117*, A04216, doi:10.1029/2011JA017268.
Winslow, R. M., B. J. Anderson, C. L. Johnson, J. A. Slavin, H. Korth, M. E. Purucker, D. N. Baker, and S. C. Solomon (2013), Mercury's magnetopause and bow shock from MESSENGER Magnetometer observations, *J. Geophys. Res. Space Physics*, *118*, 2213–2227, doi:10.1002/jgra.50237.
Xiao, C. J., Z. Y. Pu, Z. W. Ma, S. Y. Fu, Z. Y. Huang, and Q. G. Zong (2004), Inferring of flux rope orientation with the minimum variance analysis technique, *J. Geophys. Res.*, *109*, A11218, doi:10.1029/2004JA010594.
Zhang, S., A. Tian, Q. Shi, W. Sun, Z. Yao, S. Fu, Q. Zong, and Z. Pu (2016), A statistical study of the plasma sheet in the near and middle earth magnetotail [in Chinese], *Chin. J. Geophys.*, *59*(2), 411–418.
Zhong, J., W. X. Wan, J. A. Slavin, Y. Wei, R. L. Lin, L. H. Chai, J. M. Raines, Z. J. Rong, and X. H. Han (2015), Mercury's three-dimensional asymmetric magnetopause, *J. Geophys. Res. Space Physics*, *120*, 7658–7671, doi:10.1002/2015JA021425.

Zhou, X.-Z., V. Angelopoulos, J. Liu, A. Runov, and D.-X. Pan (2014), Asymmetric braking and dawnward deflection of dipolarization fronts: Effects of ion reflection, *Geophys. Res. Lett.*, *41*, 6994–7001, doi:10.1002/2014GL061794.

Zong, Q. G., et al. (1997), Geotail observations of energetic ion species and magnetic field in plasmoid-like structures in the course of an isolated substorm event, *J. Geophys. Res.*, *102*(A6), 11,409–11,428, doi:10.1029/97JA00076.

Zong, Q.-G., et al. (2004), Cluster observations of earthward flowing plasmoid in the tail, *Geophys. Res. Lett.*, *31*, L18803, doi:10.1029/2004GL020692.

Zurbuchen, T. H., et al. (2011), MESSENGER observations of the spatial distribution of planetary ions near Mercury, *Science*, *333*(6051), 1862–1865, doi:10.1126/science.1211302.